Proceedings of the VIII International Conference ION 2010, Kazimierz Dolny, Poland, June 14–17, 2010

Damage Accumulation in Nuclear Ceramics

L. Thomé[a,*], S. Moll[a,b], J. Jagielski[c], A. Debelle[a], F. Garrido[a] and G. Sattonnay[d]

[a]Centre de Spectrométrie Nucléaire et de Spectrométrie de Masse, CNRS/IN2P3, Université Paris-Sud Bât. 108, 91405 Orsay, France

[b]Pacific Northwest National Laboratory, P.O. Box 999, Richland, WA 99352, USA

[c]Institute for Electronic Materials Technology, Wólczyńska 133, 01-919 Warsaw, Poland and the Andrzej Sołtan Institute for Nuclear Studies, 05-400 Otwock/Świerk, Poland

[d]LEMHE/ICMMO, UMR 8182, Bât. 410, Université Paris-Sud, 91405 Orsay, France

Ceramics are key engineering materials in many industrial domains. The evaluation of radiation damage in ceramics placed in a radiative environment is a challenging problem for electronic, space and nuclear industries. Ion beams delivered by various types of accelerators are very efficient tools to simulate the interactions involved during the slowing-down of energetic particles. This article presents a review of the radiation effects occurring in nuclear ceramics, with an emphasis on new results concerning the damage build-up. Ions with energies in the keV–GeV range are considered for this study in order to explore both regimes of nuclear collisions (at low energy) and electronic excitations (at high energy). The recovery, by electronic excitation, of the damage created by ballistic collisions (swift heavy ion beam induced epitaxial recrystallization process) is also reported.

PACS: 61.80.−x, 61.80.Jh, 61.82.Ms, 61.43.−j, 61.85.+p, 68.37.Lp

1. Introductory remarks

Ceramics are refractory solids which possess very interesting physico-chemical properties, such as high strength, low thermal expansion, chemical stability, strong resistance against oxidation, good behavior under irradiation, etc. These materials are therefore often employed in hostile media where efficient use of energy is a prime need, e.g. extreme temperatures, corrosive surroundings, radiative environment, etc. Examples of the interest of ceramics for applications are provided by electronic, space and nuclear industries. For instance, such materials are nowadays widely used for surface coating and electronic packaging, and they are envisioned in a near future for the safe and long-term disposal of radioactive waste, and the development of inert fuel matrices for actinide transmutation. They may also be employed as cladding materials for gas-cooled fission reactors and structural components in fusion reactors. For all these applications, there is an urgent need of data concerning the behavior of nuclear ceramics upon irradiation.

The topic that is concerned here is so broad that it requires a whole book to cover the main issues; the state of knowledge was regularly upgraded in thorough reviews [1–10]. To deal it in a short article, we focus on the presentation of a few remarkable examples concerning the ion-beam modifications of nuclear ceramics (zirconia, pyrochlores, silicon carbide, etc.) with an emphasis on the mechanisms leading to damage creation and phase transformations. We report typical results obtained using advanced characterization techniques (the Rutherford backscatteringspectrometry associated to channeling (RBS/C), X-ray diffraction (XRD), transmission electron microscopy (TEM), Raman) for ceramics irradiated with ions in a broad energy range (from keV to GeV) in order to explore both nuclear collision and electronic excitation regimes.

The first section is devoted to the presentation of general considerations about the damage build-up in ion-irradiated crystals and of a new model developed to account for experimental results. The following two sections discuss the effects of elastic collisions at low energy and electronic excitations at high energy. The last section presents a new effect of crystallization by electronic excitations of the damage induced by ballistic collisions, swift heavy ion beam induced epitaxial recrystallization (called SHIBIEC).

2. General considerations about the damage build-up in ion-irradiated crystals

The topology of the damage resulting from irradiation of a crystal with low- or high-energy ions is schematically represented in Fig. 1. At low energy (below ≈ 10 keV/u), the basic process of ion energy loss is the direct transfer of energy to the atoms of the solid by elastic collisions between the projectile and the target nuclei (S_n). Along the ion path, a large fraction of primary knock-on atoms set in motion by incident ions gain a sufficient amount of energy to subsequently displace other target atoms through several secondary and higher-order collisions which lead to the creation of damage cascades (represented by ovoid objects in Fig. 1a) [11]. At high energy

* corresponding author; e-mail: thome@csnsm.in2p3.fr

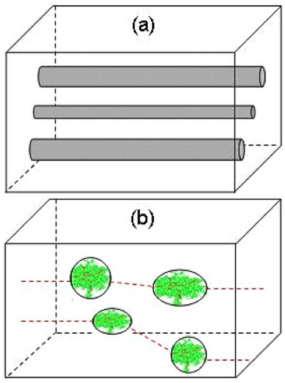

Fig. 1. Schematic representation of the damage formation in crystals irradiated with low (a) or high (b) energy ions.

(i.e. above ≈ 1 MeV/u), the electronic energy deposition (S_e) due to the passage of a swift ion induces the formation of an electrostatically unstable cylinder of ionized atoms, called latent track (represented by grey objects in Fig. 1b) [12]. The resulting atomic rearrangements may be accounted for by thermal spike [13–16] or Coulomb-explosion [17–19] mechanisms.

The first description of the damage build-up in ion-irradiated crystals was provided by Gibbons [20] which assumed that the radiation-induced damage (quantified by the parameter f_D) is due to the overlapping of a number m of ion impacts in a given volume of the target, according to the equation

$$f_D = f_D(\infty)\left[1 - \sum_{k=0}^{m-1} \frac{(\sigma_G \Phi)^k}{k!} \exp(-\sigma_G \Phi)\right], \qquad (1)$$

where $f_D(\infty)$ is the value of f_D at saturation ($f_D = 1$ for amorphization) and σ_G is the disordering cross-section. More sophisticated models (see Ref. [6]), based on a combination of direct-impact and damage-accumulation descriptions with the possibility of considering additional processes such as cascade-overlap, interface-controlled and defect-simulated mechanisms, were then elaborated to account for experimentally determined damage kinetics.

A very recent model (called multi-step damage accumulation, MSDA), based on the hypothesis that the radiation damage results from a series of successive atomic reorganizations (steps) which are triggered by microscopic or macroscopic solicitations [21], was recently developed to circumvent the drawbacks of previous descriptions. The damage accumulation follows the equation:

$$f_D = \sum_{i=1}^{n} \left(f_{D,i}^{sat} - f_{D,i-1}^{sat}\right) G\left[1 - \exp(-\sigma_i(\Phi - \Phi_{i-1}))\right], \qquad (2)$$

where n is the number of steps, $f_{D,i}^{sat}$ is the value of f_D at saturation, σ_i is the cross-section for damage formation and Φ_i is the fluence threshold, for the i-th step. G is a function which transforms negative values into 0 and leaves positive values unchanged.

3. Effects of elastic collisions at low energy

Defect cascades created by low-energy ion irradiation are responsible for a large variety of structural modifications (topological or chemical disorder, swelling, phase transformations, amorphization, etc.) which depend on several key parameters, such as the target material, the irradiation temperature, the ion fluence, flux and energy, etc.

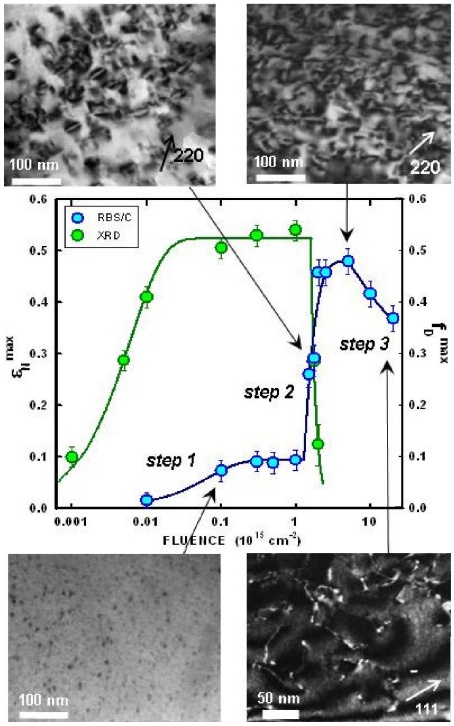

Fig. 2. Accumulated damage (f_D) and elastic strain (ε_N) vs. ion fluence for cubic zirconia crystals irradiated at RT with MeV Au ions. Solid lines are fits to data using the MSDA model [21]. Insets show TEM micrographs on samples irradiated at fluences indicated by the arrows.

A typical damage build-up, determined by RBS/C, is represented in Fig. 2 in the case of non-amorphizable materials (e.g. cubic zirconia) irradiated with MeV heavy ions [22]. The variation of the elastic strain, measured by XRD via the lattice parameter, is also represented in Fig. 2 for the same material. Both sets of data may be accounted for by using the MSDA model (lines in the figure) with a value of n which is higher than 1 in Eq. (2): $n = 3$ for RBS/C and $n = 2$ for XRD (where the strain cannot be evaluated in step 3). TEM micrographs were recorded at typical fluences (see the insets of Fig. 2). They indicate that: (i) small defect clusters, which lead to a strong increase of the elastic strain, are created during the first step; (ii) the second step is due to the formation of perfect dislocation loops and of a network of tangled dislocations, inducing a relaxation of the elastic strain and a sharp increase of f_D; (iii) long dislocations, which induce

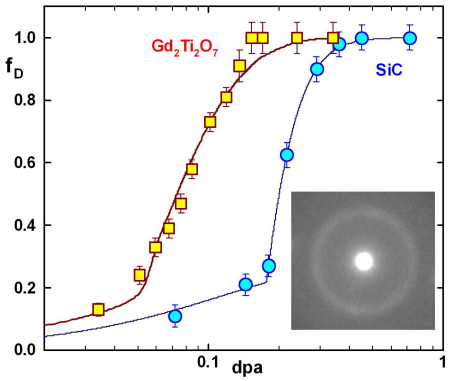

Fig. 3. Accumulated damage (f_D) vs. dose (in number of dpa) for titanate pyrochlore (squares) and silicon carbide (circles) crystals irradiated at RT with low-energy ions. The inset shows a TEM diffraction pattern on a crystal irradiated at the final fluence (indicating amorphization of the surface layer).

a reorganization of the crystal (decrease of f_D), are exhibited in step 3. A similar behavior (except step 3) was observed in cubic zirconia irradiated with a large variety of low-energy ions [22, 23], leading to the conclusion that the number of dpa is the key parameter for the evolution of the damage build-up in the nuclear collision regime. Multi-step damage accumulation processes were also reported in other non-amorphizable ceramics (for instance spinel, magnesium oxide and uranium dioxide) irradiated at low energy [24–27].

The damage build-ups, determined by RBS/C, in amorphizable ceramics also occur in several damage steps. Figure 3 illustrates this result by comparing the variation of the accumulated damage as a function of the irradiation dose (in dpa) for titanate pyrochlore (zirconate pyrochlores are generally not amorphizable) and silicon carbide crystals irradiated with MeV heavy ions [28, 29]. RBS/C data may be accounted for by using the MSDA model (lines in the figure) with $n = 2$ in Eq. (2) for the two materials. The inset shows a TEM diffraction pattern recorded at the end of irradiation, which shows that crystals are well amorphized. It is worth noting that the dose (ϕ_2) at which starts the second step of damage accumulation leading to amorphization is a parameter which reflects the stability of a material upon ion irradiation: the higher ϕ_2, the greater resistance to amorphization.

4. Effects of electronic excitation at high energy

The structure of latent tracks created in the wake of swift ions is dependent on both the ion mass (through the energy density deposited in electronic excitation) and the investigated material (insulators are generally more sensitive to S_e than semiconductors or metals).

The damage build-up, determined by RBS/C, is represented in Fig. 4 for cubic zirconia (typical of non-amorphizable materials) irradiated with GeV heavy ions [30]. The variation of the elastic strain, measured by

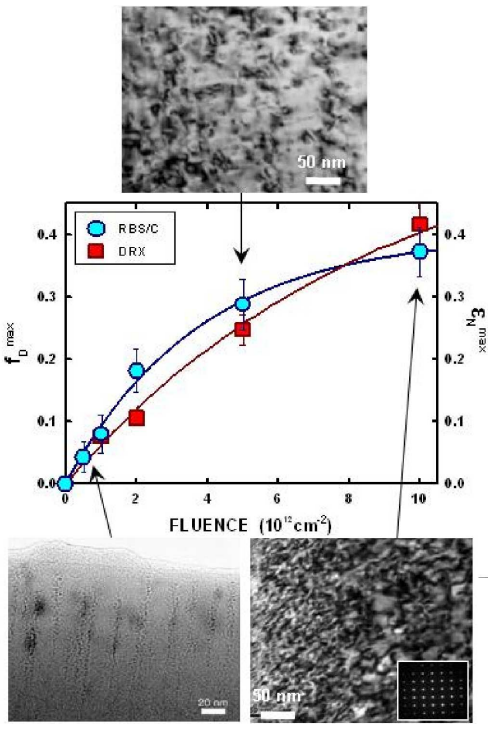

Fig. 4. Accumulated damage (f_D) and elastic strain (ε_N) vs. ion fluence for cubic zirconia crystals irradiated at RT with GeV Pb ions. Solid lines are fits to data using the MSDA model [21]. Insets show TEM micrographs on samples irradiated at fluences indicated by the arrows.

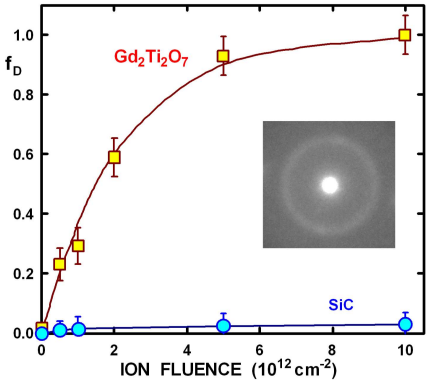

Fig. 5. Accumulated damage (f_D) vs. ion fluence for titanate pyrochlore (squares) and silicon carbide (circles) crystals irradiated at RT with high-energy ions. The inset shows a TEM diffraction pattern on a $Gd_2Ti_2O_7$ crystal irradiated at the final fluence (amorphization).

XRD, is also represented in Fig. 4 for the same material and irradiating ions. Both sets of data may be accounted for by using the MSDA model (lines in the figure) with $n = 1$ in Eq. (2). TEM micrographs, recorded at typical fluences (see the insets of Fig. 4), indicate that tracks are created at low fluences, with a microstructure which depends on the depth in the crystal. Hollow tracks (with

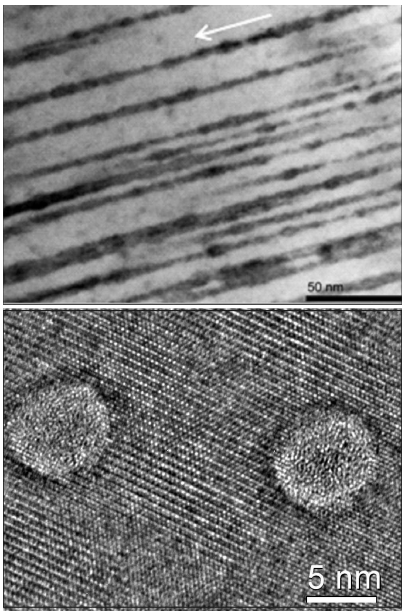

Fig. 6. TEM micrographs recorded on a $Gd_2Ti_2O_7$ crystal irradiated at RT with GeV Xe ions at 2×10^{11} cm^{-2}. Top: cross-section; bottom: plane view with a higher magnification.

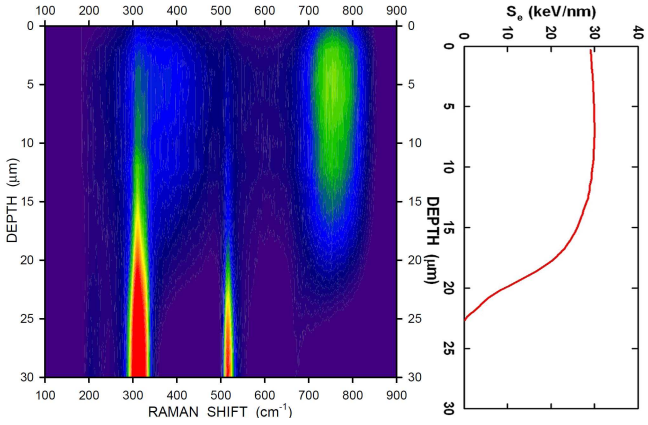

Fig. 7. Left: cartography obtained from Raman spectra recorded at different depths on a $Gd_2Ti_2O_7$ crystal irradiated at RT with GeV Xe ions at 10^{13} cm^{-2}. Right: variation with depth of the electronic energy loss (S_e) for GeV Xe ions in $Gd_2Ti_2O_7$.

a diameter of ≈ 4 nm) are observed in the subsurface region (extending up to ≈ 100 nm), together with the formation of larger hillocks (measured by atomic force microscopy (AFM)) at the surface of crystals [30]. This particular microstructure would result from a mechanism similar to the expulsion of lava from a volcano and the formation of a cone of ejected matter, due to the melting of the track core via thermal spike processes. Beyond 100 nm, filled tracks surrounded by dislocation loops are exhibited. At higher fluences (a few 10^{12} cm^{-2} for cubic zirconia), individual ion tracks overlap and the resulting microstructure is the formation of dislocation loops and of a dense network of dislocations at very high fluences (10^{13} cm^{-2} in the case of cubic zirconia). A S_e threshold for track formation, depending on the material and on the ion velocity (about 20–30 keV/nm in cubic zirconia), was found in experiments using swift heavy ions of different masses. A single-step damage accumulation process is also reported for other non-amorphizable ceramics (for instance spinel, magnesium oxide and uranium dioxide) irradiated with swift heavy ions [24–27].

Figure 5 shows the variation of the accumulated damage (determined by RBS/C) as a function of the irradiation fluence for titanate pyrochore and silicon carbide (materials which are amorphizable by elastic collisions) irradiated with GeV heavy ions [28, 29]. The behavior of both types of crystals upon electronic excitation is obviously very different. Titanate pyrochlore is amorphized (see the TEM diffraction pattern in the inset) with a damage build-up developing in a single-step process (as in the case of non-amorphizable materials), whereas almost no damage is observed in silicon carbide. Amorphization of titanate pyrochlore occurs via the formation of amorphous tracks observed by TEM (see Fig. 6). The fact that the thickness of the amorphized layer is well correlated to the S_e profile was demonstrated by the Raman results shown in Fig. 7 [31]. The vibrational mode (at 770 cm^{-1}) related to the amorphous phase is clearly seen from the surface of the sample and its intensity strongly decreases above a depth of ≈ 20 μm. In this amorphizable compound, irradiations with swift ions of different masses revealed the existence of a S_e threshold for amorphization of about 10 keV/nm [31].

5. Swift heavy ion beam induced epitaxial recrystallization

Different routes may be used to prevent amorphization or induce recrystallization of amorphous layers formed by ion irradiation. The most obvious ones are: (i) an increase of the irradiation temperature above a given threshold (of the order of 250 °C in SiC) [32–38], or (ii) thermal annealing of amorphized samples (at temperatures higher than 1000 °C in SiC) [34, 36, 39–40]. An alternative method to conventional thermal annealing to restore the crystallinity of heavily damaged crystals is the use of the ion-beam induced epitaxial crystallisation (IBIEC) process [41–43]. It consists in bombarding the samples with ion species having an energy such that the slowing down is still dominated by nuclear collisions, but with an ion projected range quite deeper than the thickness of the defective layer. An interesting feature of IBIEC in SiC is that it occurs around 300 °C [44–46], i.e. at a quite lower temperature than that required for damage recovery by thermal annealing. The use of more energetic ion beams to induce recrystallization (SHIBIEC process) [47, 48], which does not imply the same mechanisms as those prevailing at low energy, seems to be more efficient in that sense that the temperature at which recrystallization occurs by SHIBIEC is lowered as compared to that required for IBIEC.

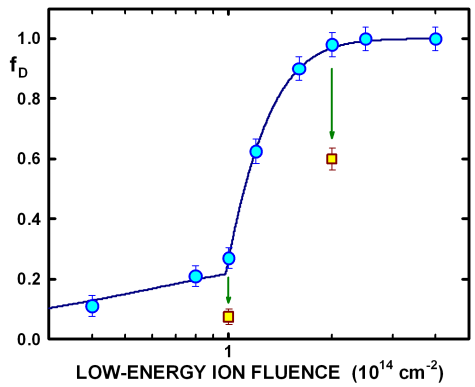

Fig. 8. Accumulated damage (f_D) vs. ion fluence for silicon carbide crystals irradiated at RT with 100 keV Fe ions (circles), and subsequently irradiated at RT (at 2×10^{13} cm^{-2}) with 870 MeV Pb ions (squares).

Figure 8 shows an example of SHIBIEC for silicon carbide [49]. The experiments involved two sequences: (i) pre-irradiation with 100 keV Fe ions at room temperature (RT) led to the progressive formation of a shallow (thickness of about 100 nm) amorphous layer (circles); (ii) post-irradiation with 870 MeV Pb ions at RT (at a fluence of 2×10^{13} cm^{-2}) induced epitaxial recrystallization by electronic energy loss (squares) of the layer which was previously amorphized by nuclear collisions. Crystallization occurs by both a decrease of the width of the initial amorphous layer and a drop of the amount of disorder measured by RBS/C (f_D). It is worth noting that an increase of the temperature at which swift heavy ion post-irradiation is performed leads to an enhancement of the SHIBIEC process.

6. Summary and future trends

Ions with energies in the keV–GeV range may be used to simulate the radiations produced in nuclear reactors or in storage forms. From a fundamental point of view such irradiations allow us exploring separately the nuclear collision and electronic excitation regimes. The damage build-up obtained in both regimes may be satisfactorily represented in the framework of a model (MSDA) which was previously developed to account for the damage production in irradiated solids. However, the shape of the build-up (particularly the number of steps which occur) and the fluence range where the damage appears strongly depend on whether nuclear collisions or electronic excitations are dominant.

At low energy, the damage distributions fit the nuclear energy deposition, a disorder peak being generally exhibited in the vicinity of the ion projected range. The defect cascades created by nuclear collisions lead to several steps of disorder accumulation, due to the formation and relaxation of radiation-induced stresses. A sharp increase of the damage is most often exhibited in the second step, associated to the creation of either dislocations for non-amorphizable materials, or an amorphous layer in the case of amorphizable materials. This second step, occurring at a dose between 0.1 and a few dpa, independently of the nature of irradiating ions, is an indicator of the radiation resistance of materials.

At high energy, the damage distributions fit the electronic energy loss, the profiles of defects being rather flat up to a depth of several micrometers. Tracks created by electronic excitation lead to a direct transformation of the melt volume into a new structure via a single-step process. Larger hillocks of matter ejected from the ion tracks are observed at the surface of irradiated crystals. The overlapping of tracks at high fluences leads to the formation of either dislocations or amorphous layers. Saturation of the damage is generally observed above a few 10^{13} cm^{-2}, i.e. fluences by almost one order of magnitude lower than those required to obtain the same amount of disorder at high energy. Results have also demonstrated the existence of a S_e threshold for track formation in the range 10–30 keV/nm, and thus the inability to damage S_e resistant materials such as silicon carbide.

Swift heavy ion irradiation of samples amorphized by nuclear collisions may lead to epitaxial recrystallization of the amorphous layer. This SHIBIEC effect differs from the well-known IBIEC process by the fact that it does not require the assistance of any external heating source. It is related to the energy deposited by the incoming ions into the target electrons and can therefore be accounted for in the framework of thermal spike models. Besides the fact that the study of the SHIBIEC process is important from a fundamental viewpoint, it presents a crucial interest for industrial applications, particularly concerning the operating cycle of nuclear reactors of the next generations. Actually, the amorphization process observed in e.g. SiC irradiated with low-energy ions and due to nuclear collisions (simulating the alpha-decay recoils or the neutron flux in a nuclear reactor) can be detrimental to the physical integrity of the material. But, since swift ions (i.e. fission fragments) are also generated in nuclear fuels, it could well happen that a balance between amorphization and damage recovery by SHIBIEC occurs in order to preserve the crystallinity of irradiated nuclear materials.

Future prospects in this research field could be the investigation of the synergy between radiation effects induced by low- and high-energy ions. Such a daunting challenge is reachable by the development of dedicated new facilities able to deliver several ion beams in a common irradiation chamber, such as the JANNUS platform running in the Orsay-Saclay area.

Acknowledgments

This work was partially financed by the GNR MATINEX. The experimental program benefited from grants provided by the French-Polish cooperation program no. 01-104.

References

[1] Hj. Matzke, *Radiat. Eff.* **64**, 3 (1982).

[2] L.W. Hobbs, F.W. Clinard Jr, S.J. Zinkle, R.C. Ewing, *J. Nucl. Mater.* **216**, 291 (1994).

[3] R.C. Ewing, W.J. Weber, F.W. Clinard Jr, *Prog. Nucl. Energy* **29**, 63 (1995).

[4] S.J. Zinkle, C. Kinoshita, *J. Nucl. Mater.* **251**, 200 (1997).

[5] C.J. Mc Hargue, *Mater. Sci. Eng. A* **253**, 94 (1998).

[6] W.J. Weber, R.C. Ewing, C.R.A. Catlow, T. Diaz de la Rubia, L.W. Hobbs, C. Kinoshita, Hj. Matzke, A.T. Motta, M. Nastasi, E.K.H. Salje, E.R. Vance, S.J. Zinkle, *J. Mater. Res.* **13**, 1434 (1998).

[7] W.L. Gong, W. Lutze, R.C. Ewing, *J. Nucl. Mater.* **277**, 239 (2000).

[8] L. Thomé, F. Garrido, *Vacuum* **63**, 619 (2001).

[9] R.C. Ewing, W.J. Weber, J. Lian, *J. Appl. Phys.* **95**, 5949 (2004).

[10] J. Lian, L.M. Wang, K. Sun, R.C. Ewing, *Microscopy Res. Tech.* **72**, 165 (2009).

[11] D.A. Thompson, *Radiat. Eff.* **56**, 105 (1981).

[12] See the Proc. of the Int. Conf. Swift Heavy Ions in Matter, *Nucl. Instrum. Methods Phys. Res. B* **267** (2009).

[13] F. Seitz, J.S. Koehler, in: *Solid State Physics: Advances in Research and Applications*, Eds. F. Seitz, D. Turnbull, Academic, New York 1956, p. 305.

[14] M. Toulemonde, C. Dufour, E. Paumier, *Phys. Rev. B* **46**, 14362 (1992).

[15] G. Szenes, *Phys. Rev. B* **51**, 8026 (1995).

[16] H. Trinkaus, A.I. Ryazanov, *Phys. Rev. Lett.* **74**, 5072 (1995).

[17] R.L. Fleischer, P.B. Price, R.M. Walker, *J. Appl. Phys.* **36**, 3645 (1965).

[18] L.E. Seiberling, J.E. Griffith, T.A. Tombrello, *Radiat. Eff.* **52**, 201 (1980).

[19] D. Lesueur, A. Dunlop, *Radiat. Eff. Def. Solids* **126**, 105 (1993).

[20] J.F. Gibbons, *IEEE* **60**, 1062 (1972).

[21] J. Jagielski, L. Thomé, *Appl. Phys. A* **97**, 147 (2009).

[22] S. Moll, L. Thomé, G. Sattonnay, A. Debelle, F. Garrido, L. Vincent, J. Jagielski, *J. Appl. Phys.* **106**, 073509 (2009).

[23] L. Thomé, J. Fradin, J. Jagielski, A. Gentils, S.E. Enescu, F. Garrido, *Europ. Phys. J. Appl. Phys.* **24**, 37 (2003).

[24] S.E. Enescu, L. Thomé, A. Gentils, T. Thomé, *J. Mater. Res.* **19**, 3463 (2004).

[25] A. Gentils, S.E. Enescu, L. Thomé, H. Khodja, G. Blaise, T. Thomé, *J. Appl. Phys.* **97**, 113509 (2005).

[26] F. Garrido, C. Choffel, J.C. Dran, L. Thomé, L. Nowicki, A. Turos, *Nucl. Instrum. Methods Phys. Res. B* **127/128**, 634 (1997).

[27] F. Garrido, L. Vincent, G. Sattonnay, L. Nowicki, L. Thomé, *Nucl. Instrum. Methods Phys. Res. B* **266**, 2842 (2008).

[28] G. Sattonnay, S. Moll, L. Thomé, C. Legros, M. Herbst-Ghysel, F. Garrido, J.M. Costantini, C. Trautmann, *Nucl. Instrum. Methods Phys. Res. B* **26**, 3043 (2008).

[29] A. Audren, A. Benyagoub, L. Thomé, F. Garrido, *Nucl. Instrum. Methods Phys. Res. B* **266**, 2810 (2008).

[30] S. Moll, L. Thomé, L. Vincent, F. Garrido, G. Sattonnay, T. Thomé, J. Jagielski, J.M. Costantini, *J. Appl. Phys.* **105**, 023512 (2009).

[31] G. Sattonnay, S. Moll, L. Thomé, C. Decorse, C. Legros, P. Simon, J. Jagielski, I. Jozwik, I. Monnet, *J. Appl. Phys.* **108**, 103512 (2010).

[32] W. Jiang, Y. Zhang, W.J. Weber, *Phys. Rev. B* **70**, 165208 (2004).

[33] E. Wendler, A. Heft, W. Wesch, *Nucl. Instrum. Methods Phys. Res. B* **141**, 105 (1998).

[34] L.L. Snead, S.J. Zinkle, J.C. Hay, M.C. Osborne, *Nucl. Instrum. Methods Phys. Res. B* **141**, 123 (1998).

[35] Y. Zhang, W.J. Weber, W. Jiang, C.M. Wang, A. Hallén, G. Possnert, *J. Appl. Phys.* **93**, 1954 (2003).

[36] V. Heera, A. Mücklich, C. Dubois, M. Voelskow, W. Skorupa, *J. Appl. Phys.* **96**, 2841 (2004).

[37] J. Slotte, K. Saarinen, M.S. Janson, A. Hallén, A.Y. Kuznetsov, B.G. Svensson, J. Wong-Leung, C. Jagadish, *J. Appl. Phys.* **97**, 033513 (2005).

[38] Y. Katoh, N. Hashimoto, S. Kondo, L.L. Snead, A. Kohyama, *J. Nucl. Mater.* **351**, 228 (2006).

[39] K. Yoshii, Y. Suzaki, A. Takeuchi, K. Yasutake, H. Kawabe, *Thin Solid Films* **199**, 85 (1991).

[40] M. Ishimaru, A. Hirata, M. Naito, In-Tae Bae, Y. Zhang, W.J. Weber, *J. Appl. Phys.* **104**, 033503 (2008).

[41] I. Golecki, G.E. Chapman, S.S. Lau, B.Y. Tsauer, J.W. Mayer, *Phys. Lett. A* **71**, 267 (1979).

[42] J. Nakata, M. Takahashi, K. Kajiyama, *Jpn. J. Appl. Phys.* **20**, 2211 (1981).

[43] J. Linnros, B. Svensson, G. Holmen, *Phys. Rev. B* **30**, 3629 (1984).

[44] V. Heera, J. Stoemenos, R. Kögler, W. Skorupa, *J. Appl. Phys.* **77**, 2999 (1995).

[45] V. Heera, R. Kögler, W. Skorupa, J. Stoemenos, *Appl. Phys. Lett.* **67**, 1999 (1995).

[46] A. Kinomura, A. Chayahara, Y. Mokuno, N. Tsubouchi, Y. Horino, *J. Appl. Phys.* **97**, 103538 (2005).

[47] T. Som, B. Satpati, O.P. Sinha, D. Kanjilal, *J. Appl. Phys.* **98**, 013532 (2005).

[48] A. Benyagoub, A. Audren, L. Thomé, F. Garrido, *Appl. Phys. Lett.* **89**, 241914 (2006).

[49] L. Thomé, A. Debelle, F. Garrido, A. Declémy, unpublished results.